Engineering Solid Mechanics12 (2024) 423-436

Contents lists available at GrowingScience

Engineering Solid Mechanics

homepage: www.GrowingScience.com/esm

Experimental determination of strain in thin aluminum plate with central hole subjected to far-field tensile loading using digital image correlation (DIC)

Angaw Chaklu Engidaw[a*], Araya Abera Betelie[b*] and Daniel Tilahun Redda[c]

[a]*M.Sc.in Mechanical Design, SMiE, AAiT, Addis Ababa University, Addis Ababa, Ethiopia*
[b]*Assistant professor of Mechanical Engineering, SMiE, AAiT, Head of Mechanical Design, Addis Ababa Institute of Technology, Addis Ababa University, Addis Ababa, Ethiopia*
[c]*Associate Professor of Mechanical Engineering/Automotive Engineering/Mechanical Design and Tribology, SMiE, AAiT, Addis Ababa University, Addis Ababa, Ethiopia*

ARTICLEINFO

Article history:
Received 12 December 2023
Accepted 11 April 2024
Available online
11 April 2024

Keywords:
Digital Image Correlation
Far-field stress
Strain
Aluminum plate
Strain gauge
VIC-3D

ABSTRACT

A flat Aluminum specimen with a geometric discontinuity, which allows testing of the applicability of 2D and 3D Digital Image Correlation Strain measurements, has been considered for this research since it is prone to high stress concentration via Addis Ababa Institute of Technology research interest. Experimental strain using digital image correlation and geometry measurements should be measured with estimated material properties and compare the results with theoretical model predictions. Aluminum plate with central hole were subjected for far field stress in the Machine shop of School of Mechanical and Industrial Engineering at Addis Ababa University in order to test the agreement between DIC's strain analysis, strain gauge strain analysis and calculated empirical formulas of strain analysis and for the stress distribution of the plate elastically deformed by using VIC-3D and strain gauge. The aim is to measure vertical strain field, Vertical strain along horizontal line through hole center as function of applied loading and vertical strain using theoretical formula along same line as measurements in a plate with central hole subjected to far field and near field tensile loading using visual image coloration (VIC-3D) software, Destensometere device and solid mechanics equations to compare strain results.

1. Introduction

Digital Image Correlation (DIC) is an optical, non- contact method for measuring full deformation across the surface of a material. Nowadays, validation of results is supported by experiments to have effective and efficient products. Digital image correlation is one of the techniques to validate results experimentally, reduce excess dimensioning of products, and give more confidence for the designer. Sheet metal is widely used in aerospace, marine and automotive engineering due to its versatility (Timoshenko, 1947; Cahill & Weatherhead, 2001; Young et al., 2002; Sciammarella & Sciammarella, 2012; Paul et al., 2018). The phenomenon of pitting corrosion in steel plates often leads to the formation of holes. The presence of these holes can cause stress, repeated stress, and reduction in strength, sudden response and changes in buckling properties (Yan et al., 2021; Milosevic et al., 2021). Localization of strain is a well-known phenomenon that occurs under various loading conditions such as uniaxial and multiaxial, monotonic and cyclic loading, as well as high-speed deformation in a broad variety of materials such as ductile single crystals, polycrystalline materials with various grain sizes down to nanocrystalline materials, and metallic glasses. Strain localizations may appear on different length scales ranging from the macroscale to the meso and microscale and can be distinguished into stationary and propagative strain localizations (Weidner & Biermann, 2021; Gu, et al., 2021; Quanjin et at., 2020; Blikharsky et al., 2022; Jordan et al., 2023). Tensile stress tends to elongate the thin aluminum by subjecting it to two equal and opposite pull forces, as a result there is an increase in length of the body. The stress, when subjected to two equal and opposites pushes, as a result of which there is decrease in length, is compressive stress (Richard et al., 2011; Hilal et al., 2011; Hannah et al., 1992; Silva et al., 2018; Engidaw et al., 2024; Chen et al., 2021; Ejiko & Olakolegun,

* Corresponding author.
E-mail addresses: Angawch1988@gmail.com (A. C. Engidaw) arsame2008@gmail.com (A.A.Betelie)

ISSN 2291-8752 (Online) - ISSN 2291-8744 (Print)

doi: 10.5267/j.esm.2024.4.002

2018; Owens et al., 2021). At the same time there is tensile strain and compressive strain. Strain gauge circuits such as wheat Son Bridge can be used for the measurements of strain values. Dummy strain gauges are positioned out-side of the specimen for temperature compensation and read zero before loading starts (Betelie et al., 2018; Wu et al., 2023; Romanowicz, et al., 2020; Ramezani, et al., 2020; He, et al., 2022; Pan et al., 2020; Mehrabian, et al., 2021). For the cantilever beam bending effect is canceled since they are equal in magnitude and opposite in direction (Young et al., 2002). Zheng et al. (2020) reported that using a simple non-contacting technique, digital image correlation (DIC) with laser speckles, to evaluate large plastic deformations of metals, especially for thin metal foils and for forming at high temperatures. The feasibility and accuracy of this DIC technique were confirmed by conducting uniaxial tensile tests using different materials. As results, the measured strains indicated a good accuracy with an error range of 6% in measuring the large plastic deformation at room temperature and 10% in measuring a large strain up to 0.6 at a high temperature of 400 °C. The strain distribution measured by DIC with laser speckles and with artificial speckles showed good agreement, confirming the feasibility of this DIC technique for measuring large plastic deformations. By using this technique, the evolution of the plastic zone was successfully investigated for thin metal sheets with a thickness of 0.5 mm. Furthermore, the strain fields involving localizations of 50 μm thick metal foils forming at room temperature and a large plastic deformation of metal tubes forming at 400 °C were evaluated qualitatively and quantitatively. Weidner and Biermann (2021) reviewed that the application of digital image correlation (DIC) for investigations of strain localization phenomena in the field of materials science and engineering (MSE) exhibiting microscopic strain localization phenomena. These investigations are supplemented by electron backscattered diffraction for interpretation of strain fields. Although DIC allows for both 2D and 3D calculations of displacement and strain fields, herein, 2D digital correlation is referred to only, as in particular with SEM only in-plane displacements are calculated so far. Rouwane et al. (2022) reported to design and validate numerically and experimentally a Digital Image Correlation (DIC) technique for the measurement of local displacement fields of samples with complex cellular geometries (samples presenting multiple random holes). It consists of a DIC method assisted with a physically sound weak regularization using an elastic B-spline image-based model. This technique introduces a separation of scales above which DIC is dominant and below which it is assisted with image-based modeling. Several in silico experimentations are performed in order to finely analyze the influence of the introduced regularization lengths for different input mechanical behaviors (elastic, elasto-plastic and geometrically non-linear) and in comparison with true error quantification. This method can estimate complex local displacement and strain fields with speckle-free low definition images, even in non-linear regimes such as local buckling or plasticity and validation was performed in 2D-DIC to allow for the comparison of the proposed method on low resolution speckle-free images with a classic DIC on speckled high resolution images. The aim of this research is to validate the DIC method for deformation and stress field variables with respect to theoretical solid mechanics and Destensometere device result in which literatures did not address till now.

2. Materials and Methods

The procedure by using digital image correlation and strain gauge, local and far field strain will be measured and compared from theoretical value as stated in the following steps.

2.1 Material Properties

Material is Aluminum T6, Loading with Single ‘Point’ load, Geometry of specimen as given below and from direct measurement, Al T6061 or T6, Young’s Modulus of 68.9GPa, poisson's ratio 0.33, Yield Stress of Al 100MPa, Strain Gauge factor 2.11 was used.

2.2 Geometry of Specimen

Specimen consists of L=203mm, W=50.7mm and thickness=2mm and hole diameter=6mm was considered.

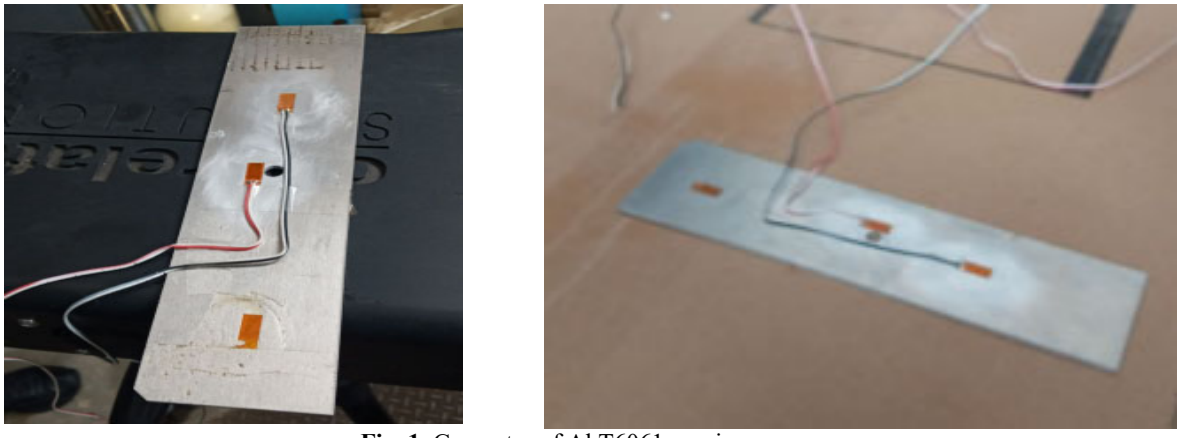

Fig. 1. Geometry of Al T6061 specimen

The specimen with strain gauge preparation starts with Selecting Al T6, strips dimensionally and drills the central hole with conventional drilling machine then makes general (dry) cleaning and locates strain gauge position on the specimen following this clean with acid intentionally and makes it one way.

Clean with water and using plaster sack the strain gauge and put on the specimen carefully. Hold with our finger for more strength with the specimen carefully. Flip the plaster and add a drop of glue between strain gauge and specimen and stick the strain gauge to specimen hardly for two minutes. Then remove the plaster cover from the strain gauge. Have small wire, flux and strain gauge now and drop small flux to wire end, strain gauge end to activate welding process then connect two wire end with two strain gauge end and weld permanently two strain gauge one near the hole and the second strain gauge 43mm away from the center of the hole to measure far field strain.

Measure at two wire end (120.8 ohm) and at the tip of strain gauge (120.2 ohm) with multi-meter and the strain gauge factor is 2.11 with 120.2 ohm value. Most common strain gauge has 350 and 120 (used strain gauge for our test) ohm value. From the two reading the difference is due to wire own resistance which generates more resistance value. For more safe measurement take care of detaching wire from the welded area. Then the specimen is ready for another task of measuring strain by applying external load. The load capacity of the tensile machine is varying up to 100kN and the test maximum allowable load of 6kN load to prevent failure of the specimen.

2.3 Speckle Images

In Vic-3D, speckle images are images or sets of images taken of a specimen as it undergoes load or motion. For this experiment speckle has been performed via the following steps

a) Have the centrally drilled rectangular shape Aluminum specimen.
b) Put in horizontal, clean and dry surface on the opposite side of strain gauge attachment.
c) Pour white powder rigorously until we have smooth white surface and give enough time to cure.
d) Pour black powder rigorously until we have good density point like black images and keep it until it cure well and grip carefully with attachment of tap at the two ends to the tensile machine.

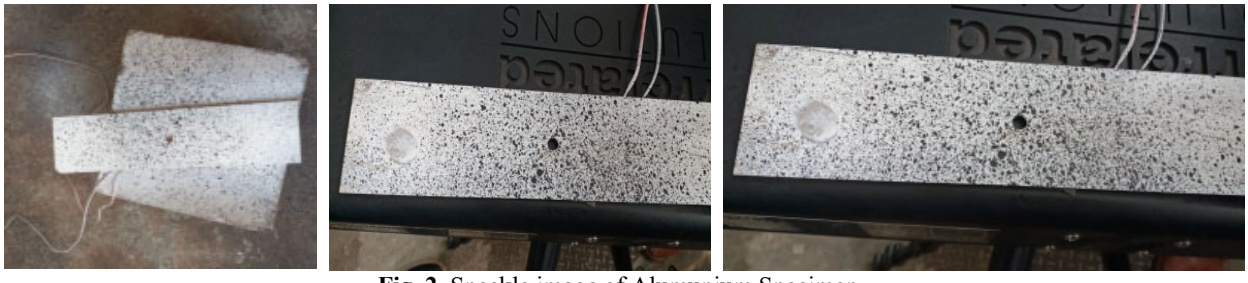

Fig. 2. Speckle image of Alumunium Specimen

2.4 Strain Gauge preparation and Data Acquisition

Mechanical testing and measurement require an understanding of the varying dynamic response of a material. The deformation that an object undergoes as a result of an applied force is known as strain which is defined as the ratio of change in length of a material to its original unaffected length as shown in Fig 3. Stress can be positive (tensile), due to elongation or negative (compressive), resulting due to contraction (Weidner & Biermann, 2021). When a material is compressed in one direction, its tendency to expand into other two directions normal to this applied force is called Poisson's effect (v). Poisson's ratio (v) is expressed as the negative ratio of strain in the transverse direction to the strain in the axial direction. Strain is dimensionless parameter and sometimes expressed in units such as in/in or mm/mm. The magnitude of the measured strain is practically very small and is often expressed as micro strain (με) which can be expressed as a force of $\varepsilon \times 10^{-6}$.

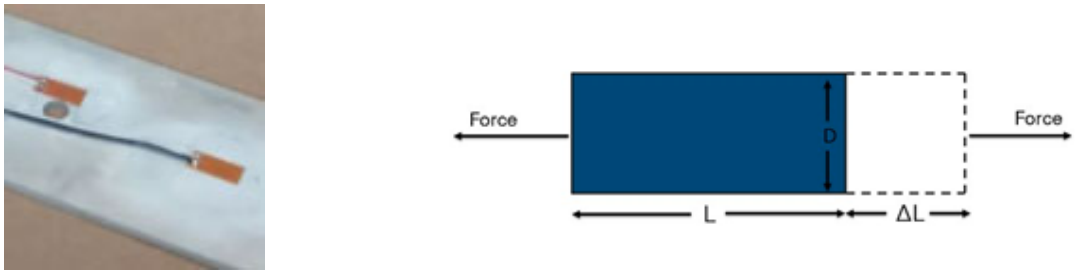

Fig. 3. Strain and strain gauge (Timoshenko, 1946; Ejiko & Olakolegun, 2018)

Strain gauge is used to measure the strain numeric value. The electrical resistance of a strain gauge changes proportionally with the applied strain. The bonded metallic strain gauge is the most widely utilized type and it comprises a grid pattern made of a fine wire or metallic foil (Quanjin et al., 2020). This grid pattern is designed to optimize the exposure of the wire or foil to strain in the parallel direction. The grid is securely bonded to a thin backing known as the carrier, which is directly attached to the test specimen. As a result any strain experienced by the test specimen is directly transferred to the strain gauge. Consequently, the strain gauge exhibits a linear alteration in electrical resistance as a response.There is a tendency to use either quarter, half or full bridge strain gauge as necessary (Blikharskyy et al., 2022; Richard et al., 2011). The quarter-bridge strain gauge is good to measure axial or bending strain with requirement of passive quarter bridge completion dummy resistor. Whereas the half bridge strain gauge is used to measure axial or bending strain. It requires half bridge completion resistors to complete the Wheatstone bridge (Engidaw et al., 2024; Chen et al., 2021; Ejiko & Olakolegun, 2018). For this strain gauge completion R4 is active strain gauge measuring tensile strain (+ε) and R3 is an active strain gauge compensating for Poisson's effect (-νε). This configuration is commonly confused with the quarter-bridge type II configuration, but type I has an active R3 element that is bonded to the strain specimen. Strain gauge measurements are able to predict strain at each point through the specimen and are unable to know critical stressed areas. If strain on each point through the specimen is required, much strain should be there. To avoid such limitation DIC technique has been introduced (Wu et al., 2023; Romanowicz et al., 2020; Yang et al., 2022; Rouwane et al.,2022) in which its measuring process has been discussed below on digital image correlation sub section (f). For the strain gauge connections first have a central hole specimen, two strain gauge plastered previously and measured dimension Al specimen. Then connect strain gauge two end wire with Destensometere device using quarter bridge, half-bridge or full- bridge connection concept. This device has an already in-built bridge connections system for 120 and 350 ohm strain gauges and quarter bridge connection is used for our case. It needs to make some adjustments to start with zero AMP, Facture (adjust gauge factor to be 2.11) and measure (adjust balance reading zero, 0.000) then it is ready to read strain if external load by the tensile machine is applied. So using the in-built bridge device strain can be measured for common strain gauge standards of 350 and 120 ohm. When the strain gauge size is small the measured value is good except that the cost to buy the strain is high. Bridge can be also connected manually using any available strain gauge and then connected with the specimen; gives zero reading in no load case. The in-built bridge device can be connected with Tektronix TDS 220 device to read graphical impact effects with time as well as to save, store, capture and process files for another purpose.

Fig. 4. Strain gauge connection procedure

2.5 Experimental Apparatus Arrangement

The whole experimental equipment for the intended DIC experiment is arranged in the SMiE workshop of having a tensile machine, VIC-3D software, camera, Tektronix TDS 220 and Destensometere device. The calibration image is required for VIC-3D and this can be obtained make the center of tensile machine gripping jaw as fixed reference, adjust the camera distance and check the additional light requirement up on looking the 14mm calibration specimen screen brightness and check that the three hole of the calibration point are shown at a time in the two camera lens (cascaded screen of the computer).

Fig. 5. VIC-2D experimental setup and machine types

If the brightness is not clear on the screen it can be adjusted by additional light, decreasing the camera distance with the tensile machine or adjusting camera focus and looking at the effect of contrast on the computer screen. If we were looking at VIC-2D no calibration image is required. Once the required brightness, the three holes at a time is shown on the cascaded window then the camera distance should be fixed and calibration image capture is started manually. The camera distance will remain fixed until all calibration images are captured and the central hole specimen is attached to the tensile machine and apply 6kN external load for far field stress and near field stress analysis completed.

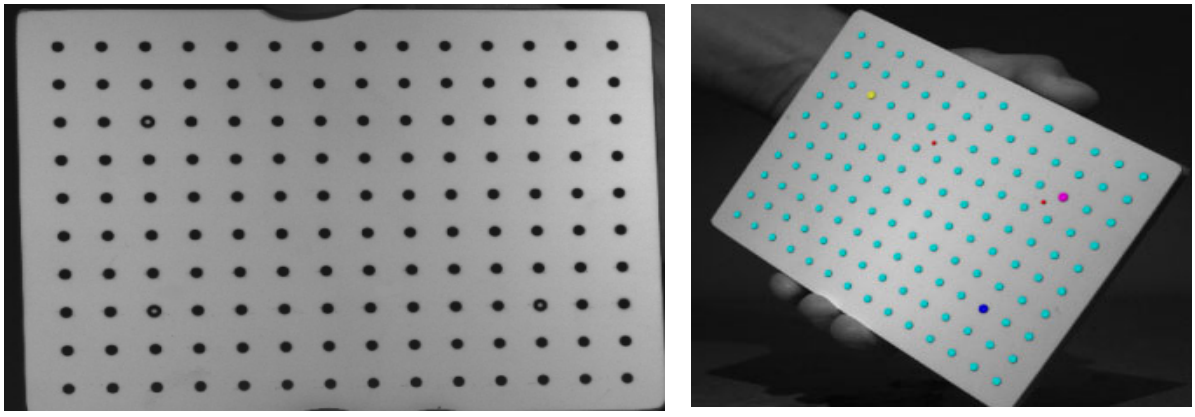

Fig. 6. Calibration plate instrument with 14mm

For this test 38 calibration images have been captured manually by rotating the calibration specimen in front, back, side, right and left, tilt in back and front ways to have good z direction strain. The operator of the calibration specimen says take/capture when he is ready and the computer expert will capture calibration images. The untargeted calibration image is filtered by the software itself during the calibration analysis. For this test the stereo system analysis score is 0.019<0.044 which is acceptable value from the VIC software manual recommendation. Then the central hole specimen is attached to the tensile machine with a tap at the two ends to prevent unnecessary slip of the specimen during tensile machine operation up to approximately 6kN. For the first test, the load was increased until it reads 5.01kN and the strain gauge connected far from the hole reads 0.074 mstrains but for the second experiment (near field strain) the load increased to 5.58kN and the strain gauge reads up to 0.083m strains. Vishay strain indicator was replaced with a strain gauge bonded far to the hole, to measure the far field strain. The first image capture activity was for the far field strain gauge connected with the Destensometere device and Tektronix TDS 220. The computer image capturing was automatic for 2 photo/second with the camera pixel capacity but starts equally with the start of the tensile machine and stops equally for the computer screen and tensile machine. Finally the test has 62 captured images for near field strain and 68 captured images for far field strain value.

2.6 Digital Image Correlation (DIC)

Accurate determination of the mechanical properties of various materials needs the application of suitable strain measurement techniques. This is crucial when dealing with loading conditions which creates complex heterogeneous deformation fields. Digital images are represented by matrices that contain the position of each pixel(x), captured at different

time instances. The incremental Digital Image Correlation (2D-DIC) technique emerged in the early 1980s as the first method of image correlation (Yang et al., 2022; Betelie et al., 2018; Chen et al., 2021). It involves using one or two cameras positioned to face the region of interest, enabling the measurement of 2D displacements. This technique also referred to as white light speckle (Zheng et al., 2020) technique, which offers the possibility to determine in-plane displacement fields at the surface of objects under any kind of loading, based on a comparison between images taken with a digital charge coupled device (CCD) camera at various load steps.

To compare two images of a specimen captured at different stages of deformation, a pixel and its corresponding mark in the original (unreformed) image are utilized. The aim is to locate the corresponding pixel in the deformed image, maximizing a predefined similarity function. This function is typically based on a least-square formulation. The mark associated with a pixel can be any distinguishing characteristics, such as its grey value, that sets it apart from other pixels in the image. A single grey value is not sufficient to uniquely identify a pixel. Therefore, in practical applications, neighboring pixels are considered. This group of pixels is referred to as a subset or correlation window. The displacement result, which is determined at the center point of the subset, represents an average of the displacements observed within the subsets pixels. The step size determines the number of pixels by which the subset is shifted in the x and y directions to calculate the next displacement result. To ensure the uniqueness of each mark, the surface must possess a non-repetitive, isotropic and highly contrasting pattern. Random speckle patterns are well suited for this purpose as they meet these requirements. By applying an arbitrary speckle pattern onto the object's surface, random speckle patterns can be generated facilitating accurate correlation based measurements (Quino et al., 2020). Multiple potential matches at different locations are examined and a similarity score is utilized to assess their quality. A classic correlation function which calculates the sum of squared differences in pixel values is employed. By utilizing an image correlation routine, it becomes possible to identify every subset of the original image within the deformed image. Consequently, the software determines the displacement values of the subset centers resulting in a complete displacement field.

3. Strain Analysis Methods

A body subjected to external forces is in a condition of both stress and strain. Stress cannot be directly measured but its effect which is change of shape of the body, involves change in the fundamental quantity, length, which can be measured thus, providing a known relationship between stress and strain; the stresses occurring in a body can be computed if sufficient strain information is available (Hassan et al., 2021; Ejiko, & Olakolegun, 2018). Strain can be analyzed using the following methods.

3.1 Strain Analysis by DIC

In order to analyze the strain results from the DIC system, we opened VIC-3D software, then speckle images were loaded and analysis of stereo system calibration gave results of 0.049, arranged subsets to 31 and steps to be 11 to get better results. Then by selecting the required surface and subtracted the hole from that surface as shown in the figure below, run the examination to get the required near field and far field strain results in x and y direction.

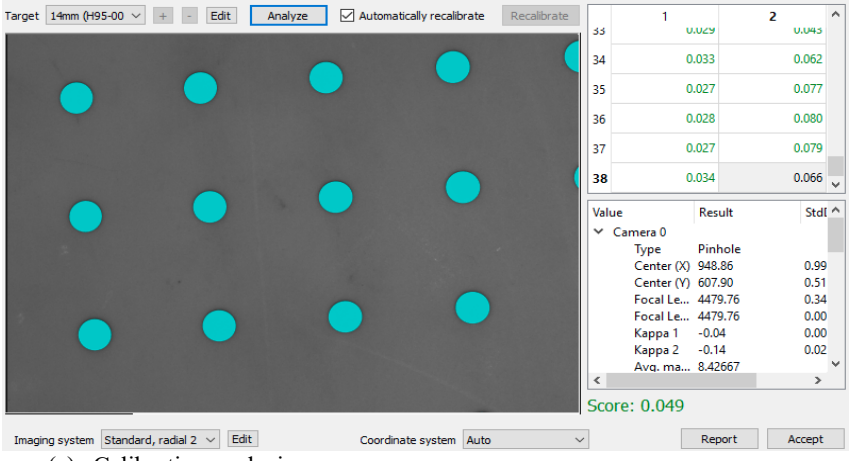

(a) Calibration analysis

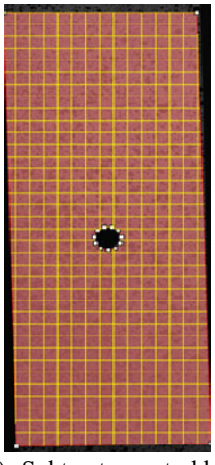

(b) Subtract a central hole

Fig. 7. Calibration analysis result and Subtraction of a central hole

As shown in Fig. 9 and Fig. 10 below, far field strain is analyzed with selection of 4 points of different direction and location Po, P_1 are along the x-axis of the hole and P_2, P_3 are along the y-axis of the hole.

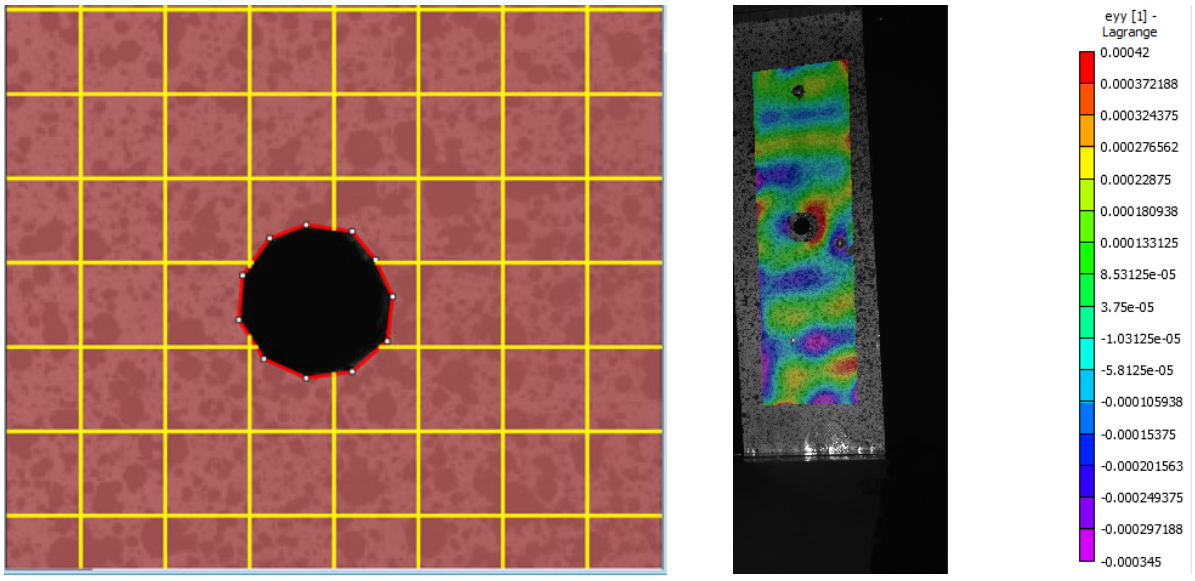

Fig. 8. Grid and Full filled strain analysis

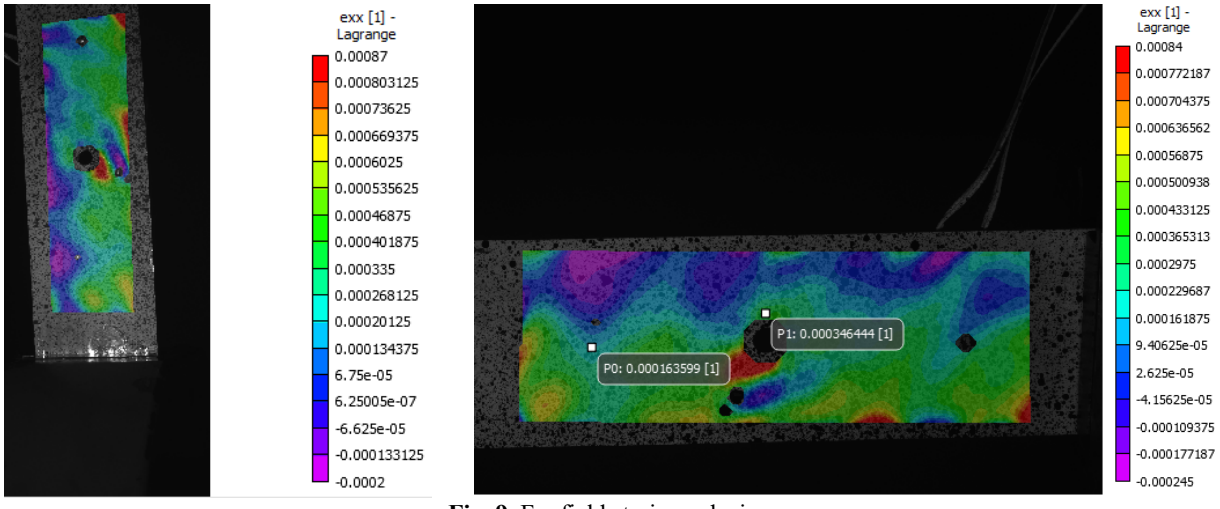

Fig. 9. Far field strain analysis

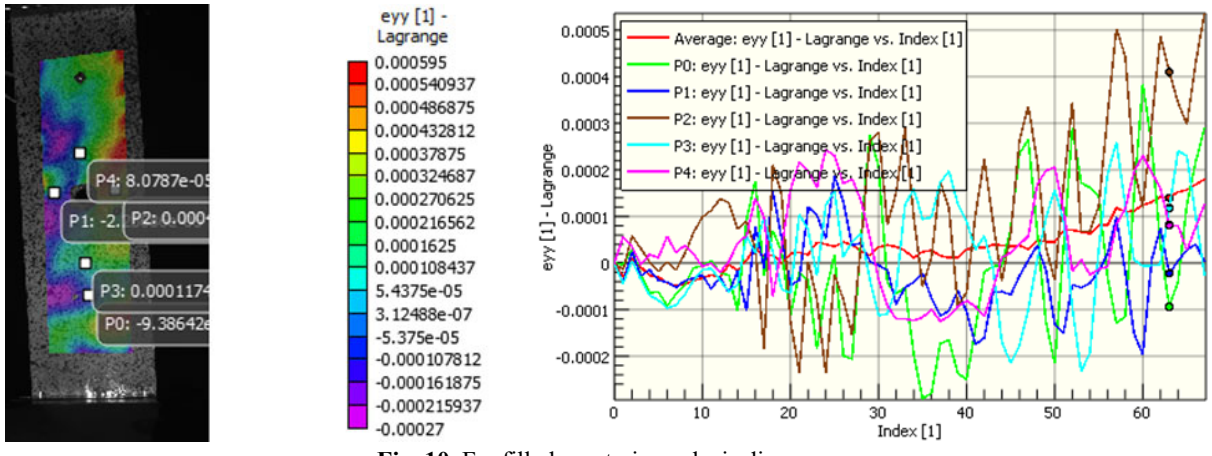

Fig. 10. Far filled e_{yy} strain analysis diagram

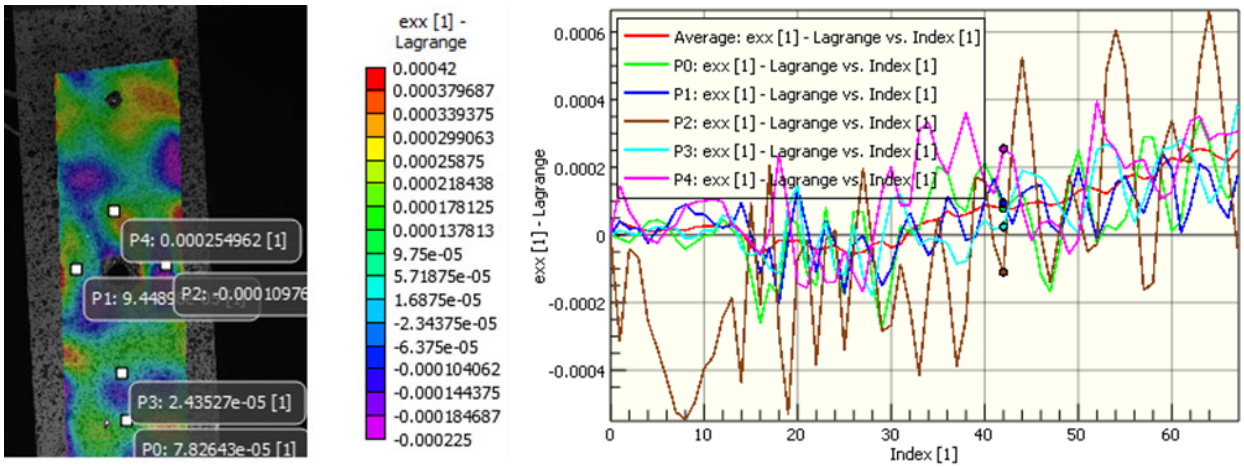

Fig. 11. Far filled e_{xx} strain analysis diagram

Far field strain along the x-axis moving to the hole increases slightly but it is almost constant throughout the x-axis as shown in Fig. 9 2D-VIC software result. The strain value in the y-axis is going to show an increased value as we move towards the hole as shown in Fig. 10. Near field strain analysis using 2D-VIC software is analyzed in Figs. 12-14 are shown below.

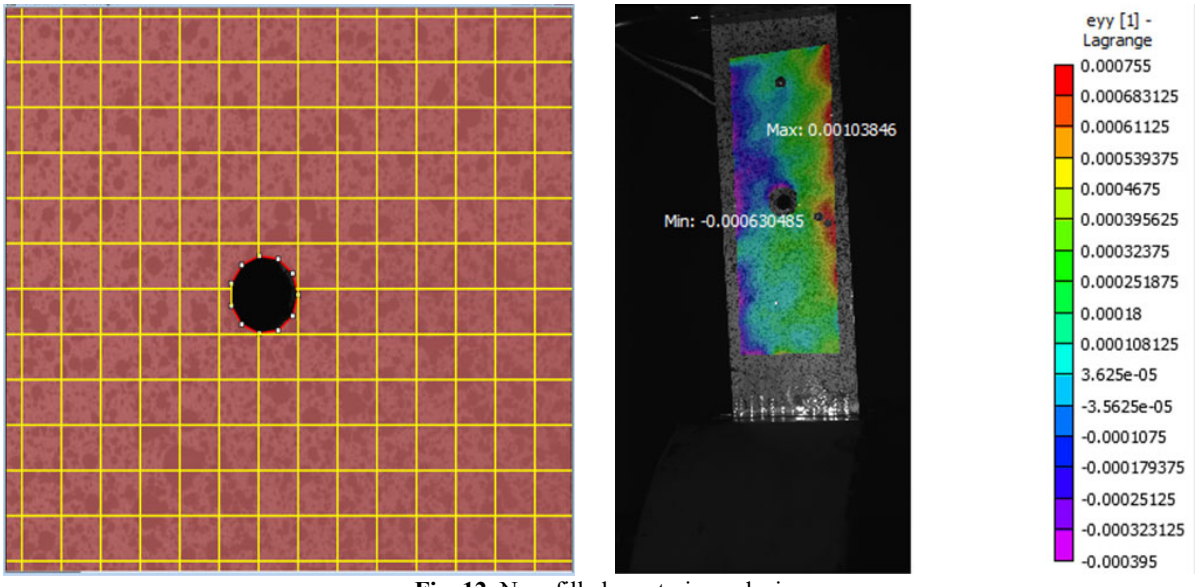

Fig. 12. Near filled e_{yy} strain analysis

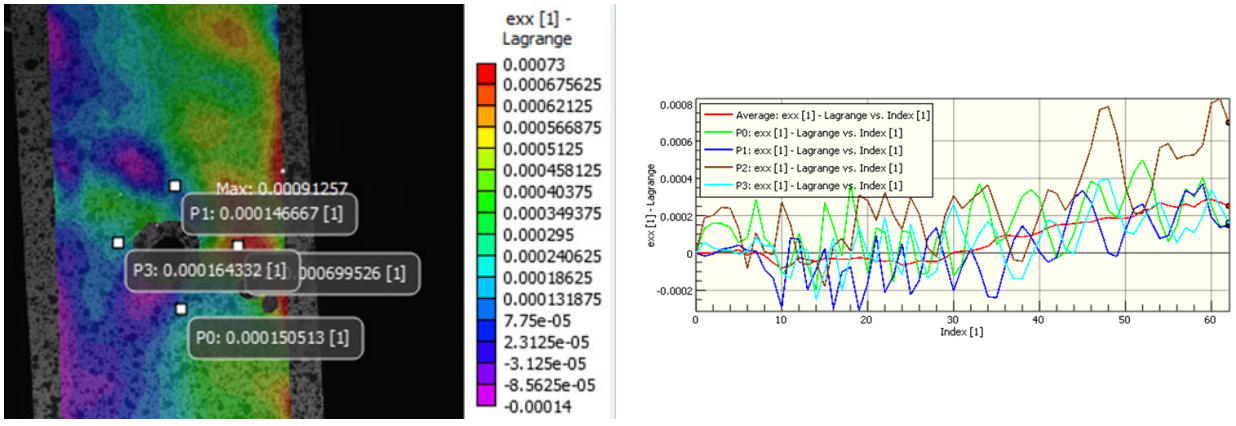

Fig. 13. Near filled e_{xx} strain analysis diagram

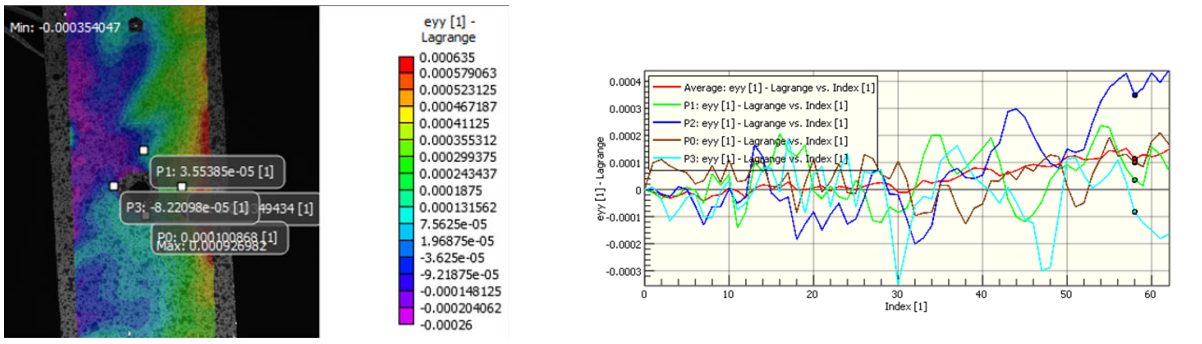

Fig. 14. Near filled e_{yy} strain analysis diagram

From the Figs. 12-14 shown above 2D-VIC software result, the near field strain along the x-axis moving to the hole increases slightly but it is almost constant throughout the x-axis. The strain value in the y-axis is going to show an increased value as we move towards the hole. Excel values for near field strain and far field strain can be extracted from the 2D-VIC software as an external file which is useful later on for intensive and detailed strain analysis.

3.2 Strain Analysis using Theoretical Solid Mechanics

If a plate with a small circular hole is subjected for a uniform tensile stress σ, there will be a high stress concentration at the point n-n (Hannah & Reed, 1992; Owens & Tippur, 2021) as shown in Fig. 15 below.

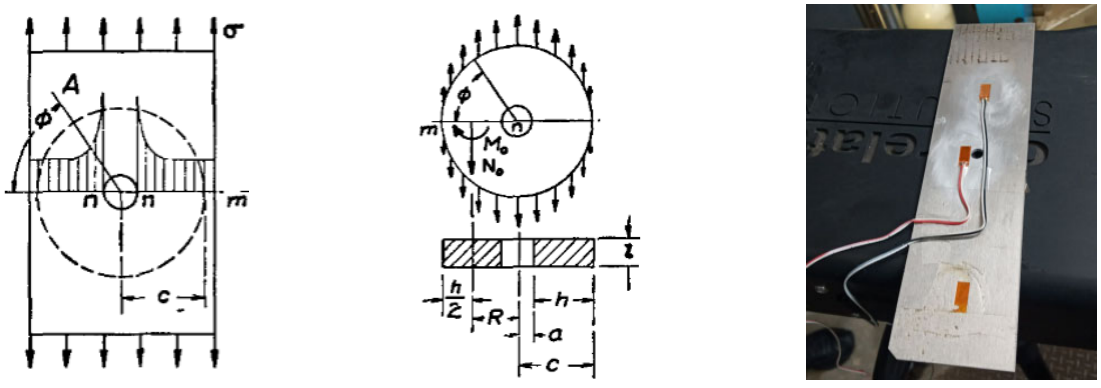

Fig. 15. Stress distribution on thin plate with hole radius **a**

Basic mechanics equation used,

$$\boldsymbol{\sigma y} = \frac{\boldsymbol{Fmax}}{\boldsymbol{[W-a]t}} \quad \text{and} \quad \boldsymbol{\varepsilon} = \frac{\boldsymbol{\sigma}}{\boldsymbol{E}} \quad \textbf{and} \quad \boldsymbol{\sigma_{Max} = \sigma_1 + \sigma_2} \tag{1}$$

At the outer surface of the ring whose radius is c, there is a vertical stress with the magnitude of $\boldsymbol{\sigma\, sin\varphi}$. The stress at point 'n' of the cross-section **mn** of the ring consists of two arts: (1) the tensile stress produced with the longitudinal force $N_o = \sigma c$ and equal to $\boldsymbol{\sigma_1 = N_o/\, h = \sigma c\, /h.}$ Bending stress produced by (M_o) which is $\boldsymbol{\sigma_2 = M_o h1/Aal a}$ where a= radius of the hole, l= distance of the neutral axis from the centroid of the cross-section and Mo= bending moment on the centroid of distance mn.

Table 1. Geometrical relation with stress (Hassan, 2021; Timoshenko, 1946)

$\frac{c}{a} =$	3	4	5	6	8	10
$\frac{2l}{h} =$	*0.1796*	*0.2238*	*0.2574*	*0.2838*	*0.3239*	*0.3536*
$\frac{\sigma_1}{\sigma} =$	**1.50**	**1.33**	**1.25**	**1.2**	**1.14**	**1.11**
$\frac{\sigma_2}{\sigma} =$	**2.33**	**1.93**	**1.83**	**1.83**	**1.95**	**2.19**
$\frac{\sigma_{max}}{\sigma} =$	**3.83**	**3.26**	**3.08**	**3.03**	**3.09**	**3.30**

Taking any point in the cross-section of the figure above mn at distance r from the center of the hole, the normal stress is given by equation

$$\boldsymbol{\sigma}_n = (\sigma \times (2 + a^2/r^2 + 3(a^4/r^4)))/2 \quad (2)$$

At point n, @ r = a, we have maximum stress $\sigma max = 3\sigma$ at $\varphi = 90\ degree$. The stress decreases rapidly as the distance increases to the edge of the plate through point n horizontally; similarly, the stress decreases rapidly as the angle increases. At $\pi/2$, the compressive stress in the tangential direction equal to the tensile stress σ applied at the end of the stress. The stress distribution can be evaluated by the theory of elasticity for the simple case of an infinitely wide plate with a small hole subjected to tensile loading. The closed form solution of stress distribution for the plate is with respect of polar coordinates (r, φ), at any point p are given by the equation below and $K_t = 3$.

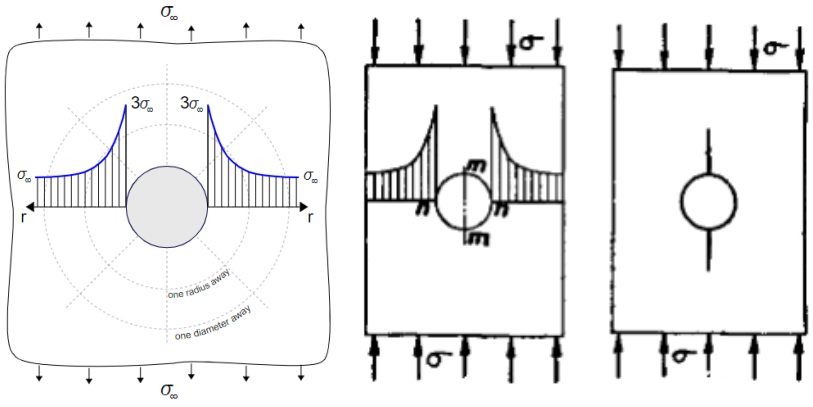

$$\sigma_{rr} = \frac{\sigma}{2}\left(1-\frac{a^2}{r^2}\right)+\frac{\sigma}{2}\left(1-\frac{a^2}{r^2}\right)\left(1-\frac{3a^2}{r^2}\right)cos2\varphi$$

$$\sigma_{\varphi\varphi} = \frac{\sigma}{2}\left(1+\frac{a^2}{r^2}\right)-\frac{\sigma}{2}\left(1+\frac{3a^2}{r^2}\right)cos2\varphi$$

$$\sigma_{r\varphi} = \frac{\sigma}{2}\left(1-\frac{a^2}{r^2}\right)\left(1+\frac{3a^2}{r^2}\right)sin2\varphi$$

Fig. 16. Stress concentration at the hole and relation of nominal, far field stress in finite plate width

Nominal stress (σ_{nom}) is the average stress of finite width plate with central hole due to the reduction in cross section. $\boldsymbol{\sigma max = \sigma Kt\frac{W}{[W-d]}}$ and stress concentration factor near the hole is $Kt = 3 - 3.14(d/W) + 3.667(d/w)^2 - 1.527(d/W)^3$

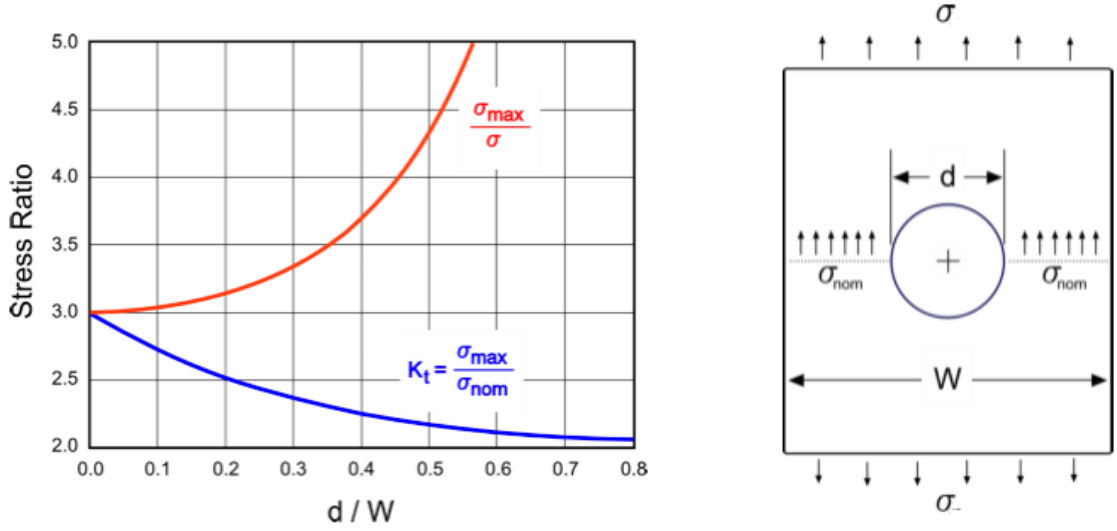

Fig. 17. Stress concentration factor graph in finite plate width (Ejiko & Olakolegun, 2018)

It needs the concept of Stress Concentration Factor (K_t) with the ratio of maximum stress to average stress as depicted above. In theory of elasticity, it is stated that stress concentration is 3σ around a circular hole and $-\sigma$ for far from the hole in an axially loaded thin infinite width plate, where the applied average stress (far field stress) $\sigma = p/wh$.

$(Yield\ Stress)\sigma y = \frac{Fmax}{[W-a]t}$ And (Far field stress) $\sigma = p/wh$ (3)

$Fmax = \sigma y \times [W - a]t$=100×10^6 Pa (50.7mm-6mm)×2mm=8940N calculated near field hole force but for our tensile machine 5.65kN (far field) and 5.61kN (near the hole) was considered.

(Far field stress) $\sigma = p/wh$= (8940N/(50.7mm×2mm)=88.1656MPa

$\sigma nom = \frac{W\sigma}{[W-d]}$= (50.7mm*88.1656*10^{6}Pa)/(50.7mm-2mm)=91.7864MPa

$Kt = 3 - 3.14(6/50.7) + 3.667(6/50.7)^2 - 1.527(6/50.7)^3 = 2.677$

$\sigma max = kt \times \sigma nom = 2.677 \times 91.7864MPa = 245.73314MPa$

$$\boldsymbol{\varepsilon} = \frac{\sigma}{E} = \left(\frac{88.1656MPa}{68.9MPa}\right) = 1.2796$$

Now using the equations generated in the polar coordinate system for the horizontal n-n direction stress distribution with zero radial and angular shear stress at any angle of these points, stress and strain for 0^0,90^0 and 180^0 is calculated and iterated. Theoretical stress result dictates that local stress is maximum at the circumference of the hole in the vertical direction, which is 3 mm radius from the center of the hole and the intensity of the stress rapidly decrease towards the magnitude of the applied far field stress of the plate which is 11.5 mm away from the center of the hole. The intensity of the angular shear stress is very small, almost near to zero, there is a noticeable radial stress at the circumference of the hole, and it gradually decreases as we move away from the circumference of the hole. The radial stress is purely tensile and the angular stress is compression with similar magnitude of the applied field stress intensity and there is no angular shear stress throughout the cross section at 0^0 in the horizontal direction. Strain calculation and iteration for $\mathbf{e_{xx}}$ and $\mathbf{e_{yy}}$ at 0^0 and 90^0 by using radial stress and hope stress respectively. So theoretical strain result dictates that local strain in the vertical-direction is raised at the circumference of the hole as similarly as that of the stress and decreases when we go away from the hole. But in the horizontal axis the strain is almost a constant compressive strain throughout the width (r).

3.3 Strain Analysis by Destensometere (Vishay) device

This is the device that reads strain value directly from the specimen when the tensile machine starts to grip and apply external load up to approximately 6kN. This has been working on the data correlation for load (kN), elongation (displacement) and strain by direct instant reading of both loading and displacement at the installed tensile machine setup operation shown in the figure 18 below.

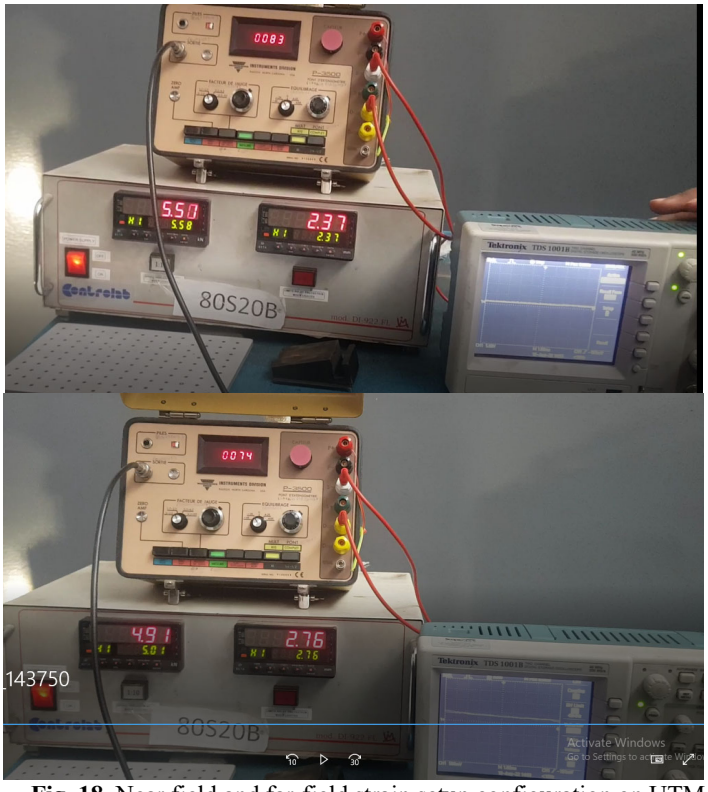

Fig. 18. Near field and far-field strain setup configuration on UTM machine

Experimental set up arrangement is different and dependant upon, either near field or far field strain connection with that of the universal testing machine (UTM) tensile machine and Vishay device.

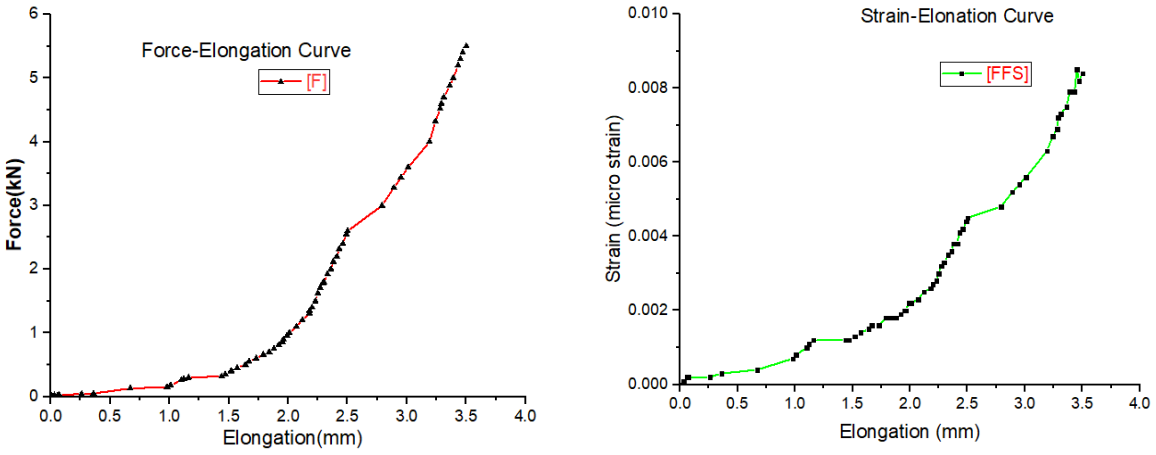

Fig. 19. Relation of force, elongation and strain using far-field strain gauge (120 ohm)

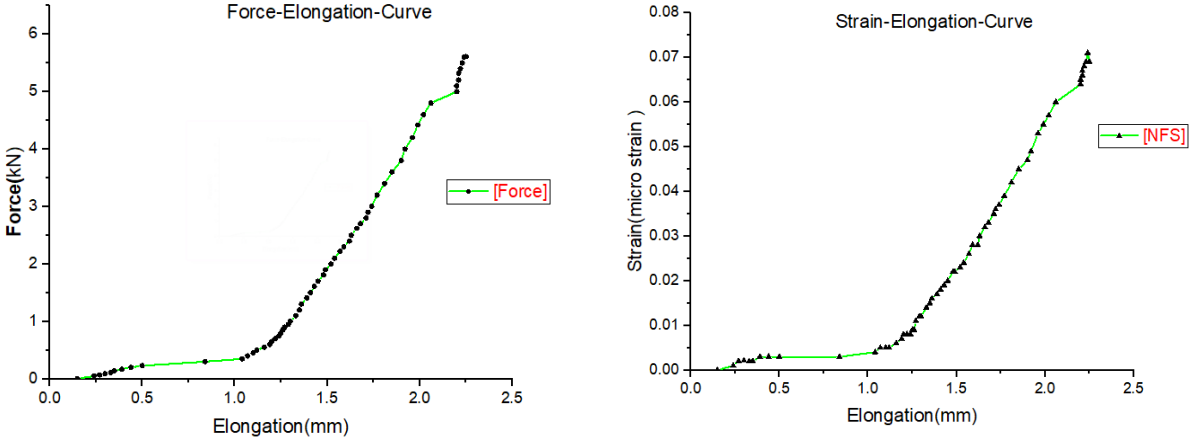

Fig. 20. Relation of force, elongation and strain using near-field strain gauge (120 ohm)

Synchronized tabulated strain, load and elongation result from direct reading. Vishay device dictates that, as the tensile machine gripping load increases, elongation is increasing as a result strain value increases. The strain is high near the hole area and decreases to be almost constant as we go away from the hole in the vertical direction for both far field and near field cases. The critical area of failure is near the hole for maximum value of the tensile gripping machine load which is 5.5kN and 5.61kN. Strain can be calculated from the elongation and original length of the specimen with increased loading. The strain value from both sides of the hole is almost equal for near field strain except for errors in well centrally gripping of the specimen.

4. Result and Discussion

Theoretically, the result was analyzed that the tensile strain near the hole is concentrated more than three times of far field strain for finite width plate as illustrated in figure 16, 17 and table 01 above. The max near field and far field strain via experiment after conducting VIC-3D software was calculated and found to be e_{yy}= 0.000926982 , e_{xx}= 0.00091257 and e_{yy}= 0.000042 , e_{xx} =0.00087 micro strain respectively. Generally as seen in the experimental curve produced by DIC is in line with G. Kirsch's formula is represented in figure 16, 17. The strain values for theoretically (e_{xx}=0.00000010708 strains for near field and e_{yy}=0.0000014538 strains for far field), direct reading from Vishay device (0.0069 micro strains for near field and 0.0084 micro strains for far field) are calculated. Far field DIC error is ((theoretical-experimental)/Theoretical) was relatively big numerical value and this is due to incorrect specimen griping, calibration error, inability to know exact position of gauge with that of the software result.

The e_{yy} result found from both experiments done by 3D-DIC technique shows, high strain concentration is seen near the hole and almost uniform and constant strain was observed far from the hole as indicated in figure. In addition, the magnitude of the local strain increased with the direct proportion of the applied load. The local compression strain e_{xx} increased, whereas the far field strains remain constant.

When the load increases, the local tensile strain increases in both experiments near the hole and it becomes maximum with direct proportion to the applied gradual load. In addition, the strain increases rapidly when reached at some point of indexes and it becomes constant after it reaches some recorded images. Far field strains that are located far from the hole are almost similar and constant in magnitude, in addition very small compression strains were observed when compared to the local strain for both experiments. High compression strain is observed near the hole in both experiments except small and constant compression strain seen far from the hole. During experiment if the camera resolution is not visible and distance of the camera to specimen is not well adjusted the captured images will not give accurate results. Specimen gripping with a universal testing machine (UTM) machine should be free from over tightening. It should also be perpendicular with the camera light rays. The specimen preparation itself should not be stressed during central hole preparation if used by a drilling machine because it creates stress concentration near the hole before UTM loading starts. The UTM machine capacity should be optimum and compatible with material types and relatively small capacity is preferred in order to avoid sensing like noise so that a sharp image and graph can be generated. Calibration image should also capture all possible degrees of freedom because it affects the inclusive interpretation of the result. Mitigation of all these limitations can decrease the errors and increase accuracy of the result.

5. Conclusion

Strain value has been measured using Vishay device, solid mechanics theoretical calculation and DIC technique, to determine full field deformation on the surface of the material. The calculation of stress and strain values through different experimental modes of measurement allowed for an understanding of measuring tools and the relationship of theoretical value with experimental value, and the associated errors. The calculation of strain for a thin aluminum plate with center hole, which was applied with tensile far field and near field stress, was done with quarter bridge strain gauge and digital image correlation methods. Among the techniques, digital image correlation is a non-contact strain measurement method and applicable for any type of geometry and material to evaluate the full field strain of the material correctly. The traditional and theoretical strain calculation is inefficient to address applicability for different material types, cannot give accurate results due to calculation error, cannot show critical failure regions of the material compared with that of DIC result. Beyond this it cannot show the strain value at any required distance on the surface of the material but DIC can do this. DIC system is versatile as it has no measurement speed limitations and avoids point based measurement results. Even though the material property is unknown, DIC can work for poisson's ratio without testing any basic mechanical property characterization. Digital image correlation results can also be further improved by correct and careful painting of the speckle, proper clamping of the specimen, good sample manufacturing with no void formation.

Conflict of Interest

This research article was done as part of the employment of authors without any sponsored funding. We have also agreed that there is no conflict of interest between the author and co-authors.

References

Betelie, A. A., Megera, Y. T., Redda, D. T., & Sinclair, A. (2018). Experimental investigation of fracture toughness for treated sisal epoxy composite. *AIMS Materials Science, 5*(1), 93-104.

Blikharskyy, Y., Kopiika, N., Khmil, R., Selejdak, J., & Blikharskyy, Z. (2022). Review of development and application of digital image correlation method for study of stress–strain state of RC Structures. *Applied Sciences, 12*(19), 10157.

Cahill, C., & Weatherhead, E. (2001). Ozone losses increase possible UV impacts in the Arctic. *Witness the Arctic: Chronicles of the NSF Arctic Sciences Program*, *8*, 1-2.

Chen, F., Bouvard, J. L., Sawada, D., Pradille, C., Hummel, M., Sixta, H., & Budtova, T. (2021). Exploring digital image correlation technique for the analysis of the tensile properties of all-cellulose composites. *Cellulose, 28*, 4165-4178.

Ejiko, S. O., & Olakolegun, O. D. (2018*). Design and Construction of Indigenous Strain Gauge Equipment*.

Engidaw, A. C., Betelie, A. A., & Redda, D. T. (2024). Extraction and characterization of nano-silica particles to enhance mechanical properties of general-purpose unsaturated polyester resin. *Science and Engineering of Composite Materials, 31*(1), 20240001.

Gu, G. H., Moon, J., Park, H. K., Kim, Y., Seo, M. H., & Kim, H. S. (2021). Obtaining a wide-strain-range true stress–strain curve using the measurement-in-neck-section method. *Experimental Mechanics, 61*(8), 1343-1348.

Hannah R. L., & Reed, S.E. (1992). “Strain Gauge user’s Manual” Society for Experimental Mechanics. P.122.

Hassan, G. M. (2021). Deformation measurement in the presence of discontinuities with digital image correlation: A review. *Optics and Lasers in Engineering, 137*, 106394

He, Z., Luo, Q., Li, Q., Zheng, G., & Sun, G. (2022). Fatigue behavior of CFRP/Al adhesive joints—Failure mechanisms study using digital image correlation (DIC) technique. *Thin-Walled Structures, 174*, 109075

Hilal, M. M., & Mohamed, S. H. (2011). A Strain Gauge Based System for Measuring Dynamic Loading on a Rotating Shaft. *International Journal of Mechanics, 5*(1), 7-38

Jordan, B., Grolleau, V., & Mohr, D. (2023). Using surround DIC to extract true stress–strain curve from uniaxial tension experiments. *International Journal of Solids and Structures, 268*, 112171.

Mehrabian, M., & Boukhili, R. (2021). 3D-DIC strain field measurements in bolted and hybrid bolted-bonded joints of woven carbon-epoxy composites. *Composites Part B: Engineering, 218*, 108875

Milošević, N. Z., Sedmak, A. S., Bakić, G. M., Lazić, V., Milošević, M., Mladenović, G., & Maslarević, A. (2021). Determination of the actual stress–strain diagram for undermatching welded joint using DIC and FEM. *Materials, 14*(16), 4691.

Owens, A. T., & Tippur, H. V. (2021). Measurement of mixed-mode fracture characteristics of an epoxy-based adhesive using a hybrid digital image correlation (DIC) and finite elements (FE) approach. *Optics and Lasers in Engineering, 140*, 106544

Pan, Z., Huang, S., Su, Y., Qiao, M., & Zhang, Q. (2020). Strain field measurements over 3000 C using 3D-Digital image correlation. *Optics and Lasers in Engineering, 127*, 105942

Paul, S. K., Roy, S., Sivaprasad, S., Bar, H. N., & Tarafder, S. (2018). Identification of post-necking tensile stress–strain behavior of steel sheet: An experimental investigation using digital image correlation technique. *Journal of Materials Engineering and Performance*, *27*, 5736-5743.

Quanjin, M., Rejab, M. R. M., Halim, Q., Merzuki, M. N. M., & Darus, M. A. H. (2020). Experimental investigation of the tensile test using digital image correlation (DIC) method. *Materials Today: Proceedings*, *27*, 757-763.

Quino, G., Chen, Y., Ramakrishnan, K. R., Martínez-Hergueta, F., Zumpano, G., Pellegrino, A., & Petrinic, N. (2020). Speckle patterns for DIC in challenging scenarios: rapid application and impact endurance. *Measurement Science and Technology, 32*(1), 015203

Ramezani, F., Ayatollahi, M. R., Akhavan-Safar, A., & Da Silva, L. F. M. (2020). A comprehensive experimental study on bi-adhesive single lap joints using DIC technique. *International Journal of Adhesion and Adhesives, 102*, 102674

Richard, S. F., & Donald, E. B (2011). *Theory and Design for Mechanical Measurements*. 5th ed. John Wiley & Sons, Inc. Chapter 11: pp. 466, 2011

Romanowicz, P. J., Szybiński, B., & Wygoda, M. (2020). Application of DIC method in the analysis of stress concentration and plastic zone development problems. *Materials*, *13*(16), 3460

Rouwane, A., Bouclier, R., Passieux, J. C., & Périé, J. N. (2022). Architecture-Driven Digital Image Correlation Technique (ADDICT) for the measurement of sub-cellular kinematic fields in speckle-free cellular materials. *International Journal of Solids and Structures, 234*, 111223

Sciammarella, C. A., & Sciammarella, F. M. (2012). *Experimental mechanics of solids*. John Wiley & Sons.

Silva, A. L., Varanis, M., Mereles, A. G., Oliveira, C., & Balthazar, J. M. (2018). A study of strain and deformation measurement using the Arduino microcontroller and strain gauges devices. *Revista Brasileira de Ensino de Física*, 41.

Timoshenko, S. (1946). *Elementary theory and problems*. Van Nostrand.

Weidner, A., & Biermann, H. (2021). Review on strain localization phenomena studied by high-resolution digital image correlation. *Advanced Engineering Materials, 23*(4), 2001409.

Wu, C. M., Kumar, S., Lin, P. C., & Chen, J. C. (2023). Strain and stress concentration of ductile composites in full-range deformation by digital image correlation. *Mechanics of Advanced Materials and Structures*, *30*(18), 3817-3825

Yan, Z., Dai, F., Liu, Y., Wei, M., & You, W. (2021). New insights into the fracture mechanism of flattened Brazilian disc specimen using digital image correlation. *Engineering Fracture Mechanics*, *252*, 107810.

Yang, R., Li, Y., Zeng, D., & Guo, P. (2022). Deep DIC: Deep learning-based digital image correlation for end-to-end displacement and strain measurement. *Journal of Materials Processing Technology, 3*02, 117474

Young, W. C., Budynas, R. G., & Sadegh, A. M. (2002). *Roark's formulas for stress and strain* (Vol. 7, pp. 125-127). New York: McGraw-hill.

Zheng, Q., Mashiwa, N., & Furushima, T. (2020). Evaluation of large plastic deformation for metals by a non-contacting technique using digital image correlation with laser speckles. Materials & Design, 191, 108626